



Enhanced Bacteriostatic Properties of Ti Alloys by Surface Nitriding

Le Fu¹ · Karthik Rajaseka² · Ioannis Katsaros² · Yihong Liu³ · Helen Wang⁴ · Håkan Engqvist² · Wei Xia²

Received: 3 January 2023 / Accepted: 8 February 2023 / Published online: 28 February 2023
© The Author(s) 2023

Abstract

Surface nitriding has been widely used to improve the surface physicochemical properties of Ti alloys. However, the currently utilized surface nitriding methods, such as laser nitriding, typically require expensive and complicated instruments, which makes surface nitriding a less cost-effective process. Meanwhile, the antibacterial properties of surface-nitrided Ti alloy implants have not been evaluated. Thereafter, in this study, we were aiming to develop an effective, simple, and cost-effective surface nitriding strategy to enhance the antimicrobial properties of Ti alloy implants. The surface nitriding strategy was realized by wet-chemical etching and thermal treatment at controlled conditions. Results showed that the above surface modification treatments exerted significant effects on the phase composition and morphology of the newly formed phases on the surface of Ti samples. Crystalline TiN and TiO₂ formed after treatments. Meanwhile, amorphous nitrides and oxynitride were also presented on the sample surfaces. The surface-modified Ti samples showed a bacterial inhibition effect compared with the non-treated Ti ones, and the bacterial inhibition effect was attributed to the released ammonia species from the surface of Ti samples. The surface modification strategy shows promise to improve the bacteriostatic property of Ti implants in dental and orthopedic fields.

Keywords Ti implant · Bacteriostatic property · Surface modification · Nitriding

Introduction

Owing to their specific high strength, low elastic modulus, excellent corrosion resistance and biocompatibility, titanium (Ti) and its alloys have been widely used as orthopaedic and dental implants for decades [1, 2]. However, pure Ti or Ti alloys typically do not exhibit antibacterial properties. Medical-device associated infection during surgery is a major and worldwide healthcare burden, leading to significant morbidity and mortality [3–5]. For example, peri-implantitis, a well-known problem in the field of dentistry across the

globe, is caused by the formation of a bacterial biofilm on the dental implant surface, which may lead to bone loss and jeopardise the longevity of the implant [6]. The first option to overcome bacterial infection was antibiotics. However, antibiotics generally have toxic side effects on the human body. Worse still, bacteria can develop resistance to antibiotics if patients take them for a long time. Taking antibiotics is not the best way to solve the problem of implant bacterial infection. Hence, there is a pressing clinical need to develop implant biomaterials that could not only promote bone tissue regeneration, but also inhibit pathogenic microorganisms [7].

People have proposed and explored several strategies to impart bacteriostatic properties to Ti alloy implants [8], among which surface modification of implant is one of the most widely used strategies [9], since surface topography and surface chemistry of implants exert significant influences on antibacterial activity. The strategies can be roughly classified into two major categories. The first strategy focuses on increasing bacteria adhesion resistance to reduce the deposition of bacteria, and it consists of utilizing chemical modifications and surface topography changes (surface roughness, charges, morphologies, etc.) to reduce

✉ Wei Xia
wei.xia@angstrom.uu.se

¹ School of Material Science and Engineering, Central South University, Changsha 410083, China

² Applied Materials Science, Department of Materials Science and Engineering, Uppsala University, 751 21 Uppsala, Sweden

³ Department of General Dentistry, Peking University School and Hospital of Stomatology, Beijing 100081, China

⁴ Department of Medical Biochemistry and Microbiology, Uppsala University, 752 37 Uppsala, Sweden

bacterial adhesion. For instance, Bello et. al has found that mono-planar nano porous Ti surface obtained by chemical etching was effective at improving osteogenic cell proliferation and increasing the focal adhesions and expression of related genes, offering great potential for osteogenic cells to adhere to implant surfaces ahead of bacteria [10].

The second approach involves functionalizing the implant surface with antimicrobial peptides, metal ions, or cytotoxic compounds to induce the death of nearby bacteria or adhered bacteria, thereby, inhibiting bacterial film formation [6, 11]. Silver ion was one of the most widely used ions to be introduced to Ti alloy implant surface through various techniques, such as magnetron sputtering [12], plasma immersion ion implantation [13], ion-assisted plasma polymerization [8], and physical vapor deposition [5]. The silver-incorporated Ti alloy implants typically showed the good antibacterial property. However, there are several issues with this strategy: first, silver ion also induces the death of healthy human cells; second, complicated instrument(s) and (or) strict experimental conditions are needed to introduce silver ions to Ti alloy implants. For instance, for the magnetron sputtering strategy [12] a magnetron sputter operating at high voltage or high current is needed. Meanwhile, contaminations may also take place via the deposition of materials from the plasma container (e.g., Fe and Si) or inappropriate processing parameters [14]. Sputtering and ion implantation techniques typically show low processing rates and inferior flexibility, which limits their application to manufacture the workpieces with complicated shape and precise dimensional tolerance.

Surface nitriding is an effective method to improve the tribological properties and corrosion resistance of Ti alloys due to the fact that nitrided layers exhibit high hardness, good thermal and chemical stability, and high wear resistance [15, 16]. In the field of biomaterials, researchers have found that nitrided layers intrinsically or deliberately formed on the surface of biomaterials showed antibacterial properties. Pezzotti et al. observed a buffering effect via the formation of ammonium ions (NH_4^+) and their modifications on the surface of Si_3N_4 [17]. This effect could induce chemically driven lysis of porphyrymonas gingivalis through a feeding and poisoning mechanism. Meanwhile, the author also found that the reactive nitrogen species (RNS) inhibited the adhesion and activity of surface bacteria, since RNS such as N_2O , NO , and OONO^- were highly effective biocides [18]. The antibacterial effects of nitrided layers on the surface of biomaterials have also been verified by other researchers [19–21]. A few studies focusing on improving the antibacterial properties of Ti alloys via surface nitriding have been conducted. For instance, $\text{Ti}_6\text{Al}_4\text{V}$ alloy was laser-nitrided in the open-air by Chan et al. [22], and they found that wear particles from the laser-nitrided surfaces displayed anti-microbial properties against *S. aureus*, compared with

those from the base metal surfaces. Donaghy et al. reported that the laser-nitrided Ti-35Nb-7Zr-6Ta alloy showed drastically reduced bacterial attachment compared with the control group without surface nitriding [23]. And, they attributed the antibacterial properties to the hydrophilic nature of the laser-nitrided surfaces. Although surface nitriding is an effective strategy to improve the antibacterial properties of Ti alloys, the reported surface nitriding processes, such as gas nitriding, plasma nitriding, and laser nitriding, usually require specific and expensive instruments and hours of treatment time [8, 23, 24]. Thereby, it is of great significance to develop an effective, simple, as well as cost-effective method to achieve surface nitriding of Ti alloys. In this study, we were aiming to nitride the surface of Ti alloys through wet-chemical etching and heat-treatment at controlled conditions. The effects of etching and heat-treatment parameters on the phase composition and morphology of Ti alloys have been explored. In addition, the antibacterial properties of the surface-modified Ti have been evaluated.

Materials and Methods

Materials Design Concept

A schematic diagram of the material design concept of the antibacterial Ti alloy biomaterials is shown in Fig. 1. First, polished Ti alloy was soaked in alkaline solution for a certain time. The purpose of this step is to remove the surface oxide layer, since typically there is a very thin protective oxide layer on the surface of Ti alloy. Meanwhile, Ti would react with alkaline solution to form a thin layer of titanate (Step I), which shows porous morphology. Second, the Ti alloy was heat treated in an N_2 atmosphere to form a silicon oxynitride layer (Step II). The porous titanate layer could increase the surface area of Ti surface, which is beneficial to the nitrogenization reaction. Third, once the surface-modified Ti alloy was implanted into the human body. Oxynitride present on the Ti surface would react with H_2O in human fluid and release ammonia (Step III). Many studies have demonstrated that ammonia is unfavorable for bacterial adhesion [25, 26]. The release of ammonia to the surrounding tissue of the Ti implant would thereby impart bacteriostatic properties to the surface-modified Ti implant.

Wet-Chemical Etching and Heat-Treatments

Grade 2 titanium (Ti) discs were polished with waterproof silicon carbide polishing paper to create smooth and uniformly polished surfaces. Wet-chemical etching was utilized to create a special surface chemistry and surface topology on the Ti discs. The polished discs were ultrasonicated for 5 min in 20 ml of deionized water to wash away the

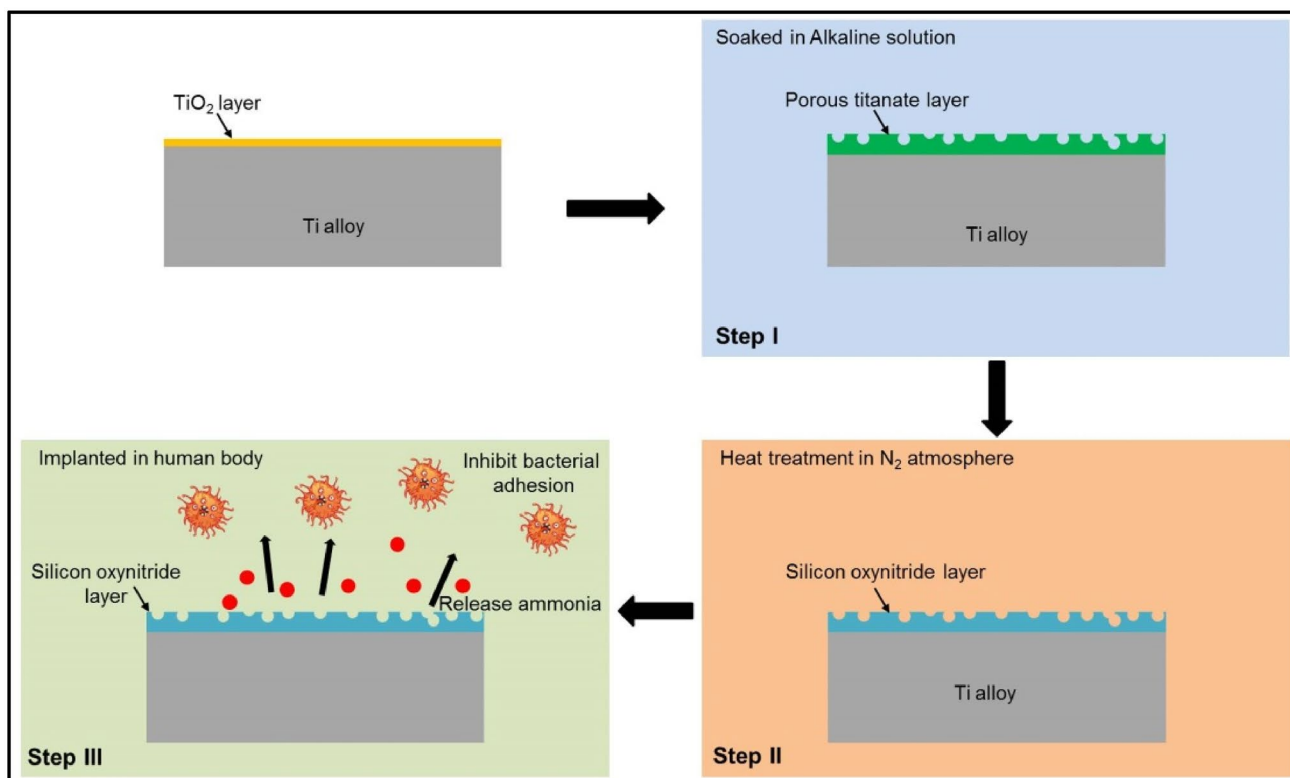


Fig. 1 Schematic diagram of the material design concept of the antibacterial Ti alloy biomaterials. Step I: Ti alloy plate with a thin layer of TiO_2 is soaked in an alkaline solution to form a thin layer of titanate that shows porous morphology; Step II: Ti alloy plate is heat treated in an N_2 atmosphere to form silicon oxynitride layer (nitro-

genization reaction); Step III: Once the surface-modified Ti alloy plate is implanted into human body. Silicon oxynitride present on the Ti surface would react with H_2O in human fluid and release ammonia, which is unfavorable for bacterial adhesion

loosened impurities. The discs were placed in a glass beaker with the polished surface on the top and stored at 37°C to facilitate drying of the discs. The polished and dried discs were soaked in several different combinations of solvents consisting of sodium silicate (pure solution, reagent grade from Sigma-Aldrich), ammonium hydroxide (ACS reagent, 28–30% NH_3 basis from Sigma-Aldrich) and sodium hydroxide (extremely pure, 98–100.5% pellets from Sigma-Aldrich). A series of tests with varying temperatures, volumes, and soaking time were conducted in order to obtain the desired chemical reaction. At the end of the soaking process, each sample disc is gently washed with approximately 15 ml of running deionized water. This was to ensure that there was no excess chemical residue on the surface of the disc. While we were cautious not to wash away any desired compound that may have been formed on the sample surface. Heat-treatments of the etched samples were conducted in a tube furnace at different temperatures for varying durations. To facilitate the occurrence of nitrogenization reactions on Ti disc surfaces, the tube furnace was connected with flowing nitrogen (N_2) gas. The ramping rate was set as $8^\circ\text{C}/\text{min}$. After the dwelling stage, the samples were cooled

down to room temperature at the natural pace in the tube furnace. Different wet-chemical etching and thermal treatment parameters have been explored to investigate their effects on the surface morphologies and bacteriostatic properties of Ti alloy. The parameters are summarized in Table 1.

Material Characterizations

Grazing incidence X-ray diffraction measurements were conducted to evaluate the surface phase composition of the treated Ti alloy. The measurements were performed on a parallel beam geometry X-ray diffractometer (Siemens, Diffractometer D5000) with an incidence angle of 5° and a step size of 0.02° . The scan was run between 10° and 80° . The scan speed was set as 3 s per step. The surface morphology of the Ti samples was examined by field-emission scanning electron microscopy (SEM) (Merlin, Zeiss, Germany). The voltage and current for SEM measurements were 5 kV and 10 nA, respectively. The elemental information on the top surface was determined by X-ray photoelectron spectroscopy (XPS, Physical Electronics Quantum 2000, Al $\text{K}\alpha$ X-ray source). During measurement, ion and electron gun were

Table 1 Wet-chemical etching and heat-treatment parameters of the Ti discs

Sample	Wet-chemical etching			Heat-treatment	
	Solution	Soaking temperature (°C)	Soaking time (h)	Dwelling temperature (°C)	Dwelling time (h)
T1	SS + NH (1:1 volume ratio)	60	24	1000	10
T2	SS + AS (1:1 volume ratio)	60	24	1000	10
T3	SS	37	72	800	2
T4	SS + AS (1:4 volume ratio)	60	120	500	24

SS sodium silicate; AS ammonia solution; NH NaOH solution

turned on during measurements to neutralize the surface charge build-up and the spectral energies were calibrated by setting the binding energy of the C–C as a reference at 285.0 eV. Data analysis was performed using the MultiPak software (Physical Electronics).

Colony Forming Units

The bacterial strain selected for the antibacterial study was Gram-positive bacteria, *Staphylococcus epidermis* (XEN 43). This is because Gram-positive bacteria are the most common and virulent pathogens involved in biomaterial-associated infection in the clinic [8]. These bacteria adhere to the surface of the implant, multiply and produce a slime called biofilm. This polymeric film encapsulates the pathogens, protecting them against the host response and antimicrobial agents. There is a pressing clinical need to develop Ti alloy implants that show resistance to Gram-positive bacteria. 10 µl of the frozen bacterial cells were first streaked onto an agar plate and grown overnight. Then, fresh colonies were taken from the plate and added to 10 ml of Lysogeny (Luria) Broth (LB). The bacterial suspension was incubated at 37 °C overnight. 100 µl of the overnight bacterial culture was once again diluted in 10 ml of fresh LB media and incubated at 37 °C for 4 h. Double incubation ensures a new generation of active cells is obtained. After 4 h of incubation, the optical density was measured on a UV spectrophotometer at a wavelength of 600 nm. The optical density was then adjusted to 0.3. Samples were autoclaved at 120 °C before tests. The sterilized samples were then carefully placed into a 24-well culture plate with the heat-treated side facing upwards, followed by seeding 10 µl of the bacterial suspension on the surface of the sterilized Ti samples. The remaining empty wells were filled with 600 µl of ultrapure water (MilliQ) to minimize evaporation of the bacterial suspension. The 24-well plate with the samples was then incubated at 37 °C for 1.5 h in an incubator. After incubation, 1 ml of Phosphate Buffered Saline (PBS) solution was added to the wells containing the samples and then extracted in order to remove the non-adherent bacteria. The PBS was added along the empty space in the sample's well to avoid washing away of any adherent cells. The addition and extraction of PBS was

done twice. Each sample was then carefully transferred into tubes filled with 1 ml PBS. The tubes were then vortexed for 60 s to detach and resuspend the adhered bacteria from the discs into the PBS. After that, 100 µl of the bacterial-PBS suspension was plated directly to obtain 1 × concentration of the cells, followed by plating ten-fold (10 ×) and 100-fold (100 ×) serial dilutions of the bacterial-PBS suspension onto LB agar plates. The plates were incubated at 37 °C for 18 h in an incubator. The number of colonies present on the 100 times dilution plates were qualitatively measured and compared with that of the control group.

Results and Discussion

Surface Morphologies and Phase Composition

SEM images of Sample T1 are demonstrated in Fig. 2. Sample T1 was etched in a mixture of sodium silicate and NaOH solution at 60 °C for 24 h, followed by thermal treatment at 1000 °C for 10 h (Table 1). As can be seen Fig. 2a, both deep scratches (indicated by white arrows) and some fragments (indicated by blue arrows) can be clearly observed on the surface. The scratches were caused by grinding and polishing. The fragments could be Ti alloy itself, or it could be the products of the chemical reaction between Ti alloy and the mixture of sodium silicate and NaOH solution. After thermal treatment, distinct surface morphology changes occurred, with the formation of both rod-like (Fig. 2b, marked by red arrows) and near-spherical (Fig. 2c, marked by the yellow cycle) particles at two different regions. The sizes of both the rod-like and near-spherical particles were on nanoscale. By comparing the surface morphologies of Sample T1 before (Fig. 2a) and after thermal treatment (Fig. 2b, c), it is clear that nitro-genization occurred during the thermal treatment in the N₂ atmosphere. Meanwhile, at the region marked by the blue cycle in Fig. 2c the near-spherical nanoparticles were connected, which was different from the region marked by the yellow cycle, where the nanoparticles were isolated. Due to the formation of the nanoparticles, the surface roughness and surface area of the Ti disc increased.

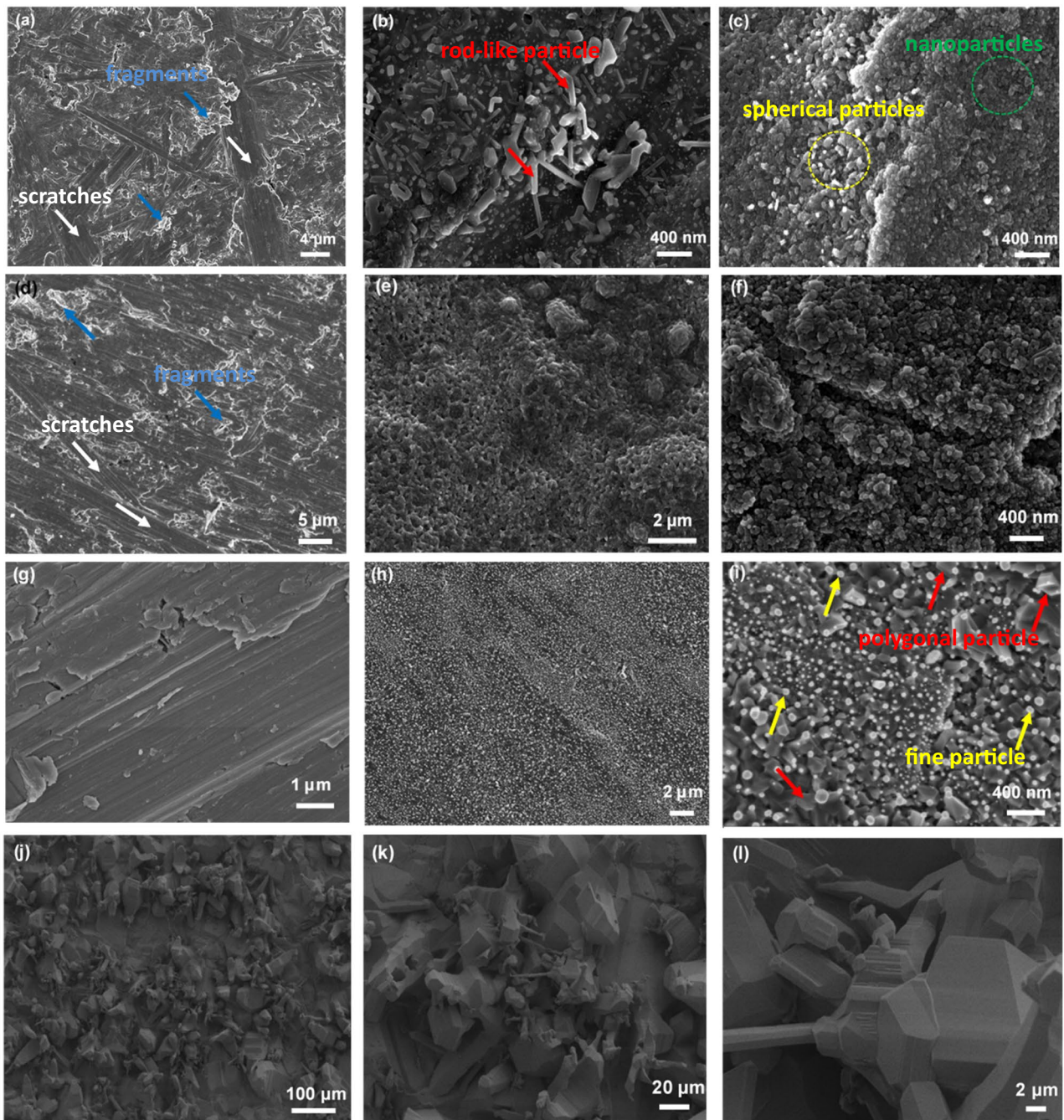


Fig. 2 Surface morphologies of the Ti discs. Sample T1: **a** after wet-chemical etching in a mixture of sodium silicate and NaOH solution. **b, c** after thermal treatment at 1000 °C for 2 h at two different regions, respectively. Sample T2: **d** after wet-chemical etching in a mixture solution of sodium silicate and ammonia solution; **e, f** after thermal treating at 1000 °C for 10 h at low magnification and high

magnification, respectively. Sample T3: **g** after chemical etching in sodium silicate solution at low magnification and high magnification, respectively; **h, i** after thermal treatment at 800 °C for 2 h at low magnification and high magnification, respectively. Sample T4: **j** after wet-chemical etching; **k, l** after thermal treatment at 1000 °C for 10 h at low magnification and high magnification, respectively

The Ti disc obtained certain surface topography after chemical etching and thermal treatment, which could be beneficial to protein adsorption and cell adhesion once the material was implanted into the human body [4, 10]. For Sample T2, both scratches (indicated by white arrows)

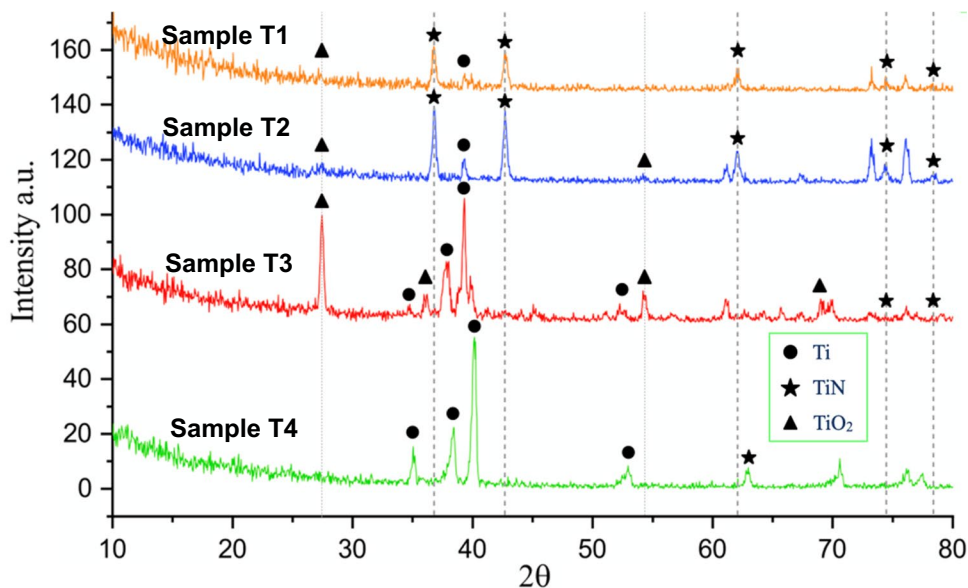
caused by grinding and polishing and fragments (indicated by blue arrows) can be clearly observed on the sample surface, which was very similar to those of the Sample T1 (Fig. 2d). After thermal treatment, a porous surface topography was formed with large several nanosized

pores (Fig. 2e). A closer inspection of the porous surface revealed that the porous surface consisted of nanoparticles with homogenous size distribution (Fig. 2f). There were no significant differences between Sample T3 (Fig. 2g) and Sample T1 and T2 after chemical etching. However, surface morphologies of Sample T3 (Fig. 2h, i) were totally different from those of Sample T1 and T2 after thermal treatment in the N_2 atmosphere. The surface of Sample T3 was covered by a large number of particles (Fig. 2h). Some particles had polygonal morphology and their sizes were approximately 200 nm (marked by red arrows, Fig. 2i). There were also some very fine particles, as indicated by yellow arrows. They had spherical morphology and their sizes were smaller than 100 nm. Surface morphologies of Sample T4 were also observed with SEM and the results were shown in Fig. 2j–l, from which it can be seen that the sample surface was also covered by particles with polygonal morphology (Fig. 2j). At higher magnification (Fig. 2k, l), it can be observed that the particles had sharp edges and flat surfaces, meanwhile, their sizes were in the scale of dozens of microns. The surface of Ti alloys after laser nitriding were typically fully covered by laser tracks and micron TiN particles were formed on the surfaces [22, 27]. It is difficult to alter the surface morphologies of the laser-nitrided Ti alloy. In comparison, as can be seen in Fig. 2 different surface morphologies can be obtained in our study by changing the processing parameters. This is one of the advantages of our strategy (chemical etching and thermal treatment) over laser nitriding, since it is well-acknowledged that cell and bacterial adhesion on implant surface are affected greatly by surface morphology [11, 28]. In our case, it is possible to obtain an optimum surface that is beneficial to cell adhesion while adverse to

the bacterial adhesion by changing the chemical etching and (or) thermal treatment parameters.

Grazing incidence X-ray diffraction (GIXRD) was utilized to investigate the surface crystallographic structure [29]. The GIXRD patterns of surface-modified Ti discs are demonstrated in Fig. 3, from which it can be seen that on the surface of Sample T1 crystalline TiN and a small amount of TiO_2 were formed after surface modification treatments. Meanwhile, weak peaks of Ti can also be observed, which could be because the surface layer formed by surface modification treatments was very thin, so that GIXRD also detected the information of the Ti substrate. The surface phase composition of Sample T2 was very close to that of the Sample T1 (Fig. 3). In comparison, the surface of Sample T3 was predominately composed of TiO_2 and Ti. For Sample T4, Ti peaks were strong, and weak peaks of TiN were also detected (Fig. 2). GIXRD result of Sample T2 showed that the surface was predominately composed of crystalline TiN. Thus, it is highly possible that the nanoparticles (Fig. 2f) on the surface of Sample T2 were TiN nanoparticles. The difference between Sample T1 and Sample T2 in terms of surface modification process is that Sample T1 was soaked in sodium silicate and NaOH solution, while Sample T2 was soaked in sodium silicate and ammonia solution. Hence, the selection of an etching chemical solution exerts the significant effect of the surface morphologies of the sample. From the GIXRD result (Fig. 3), no other crystalline phase was formed on the surface of Sample T4, except Ti. The dwelling temperature of Sample T3 and T4 were 800 °C and 500 °C, respectively, which was lower than that of Sample T1 and T2 (1000 °C). Rodriguez et al. conducted solar nitriding on Ti6Al4V alloys and they found that a thin porous layer of TiN appeared at the surface after nitriding at 1250 °C for

Fig. 3 GI-XRD patterns of the surfaced modified Ti alloy



3 h [15]. With the increase of nitriding time (to 5 h and 8 h), $\text{TiO}_{0.34}\text{N}_{0.74}$ was formed. In this study, we did not detect the formation of $\text{TiO}_{0.34}\text{N}_{0.74}$ from the GIXRD results (Fig. 2). This is because nitriding process is controlled by the diffusion of nitrogen through the Ti surface. The thermal treatment temperature of our study (800 °C or 1000 °C) is lower than that of the reported one (1250 °C) [15], so it is more difficult for nitrogen to penetrate the surface layer and form titanium oxynitride. Based on the above SEM and GIXRD results, it can be concluded that the parameters of surface modification treatments exert significant influences on phase composition and morphologies of the newly formed phases on the sample surfaces.

Surface Chemical Composition

GIXRD can only detect crystalline phases formed on the sample surface, while it is possible that some amorphous phases could also form on the surfaces after treatment. Hence, the XPS technique was applied to detect the chemical composition of the sample and the result is shown in Fig. 4. It can be observed from the survey spectrum (Fig. 4a) that Ti, O, C, N, and Si elements were detected on the surface of Sample T1. The presence of Si element could be because of the residual etching chemicals, since Sample T1 was immersed in a mixture of sodium silicate and NaOH solution. The presence of the C 1 s peak could be because the sample was contaminated during sample preparation, or a small amount of C element in the atmosphere was absorbed on the sample surface. Ti signals were detected, which could be attributed to the formed crystalline TiN phase (Fig. 3). High-resolution spectrums of N 1 s and O 1 s are demonstrated in Fig. 4b and c, respectively. The measured peak (black line) of N 1 s in the Sample T1 can be deconvoluted into two separate peaks which are centralized at 396.35 eV (red line) and 397.04 eV (green line), respectively. N element could form a bond with Ti and O element, i.e., Ti-N bond and N-O bond, respectively. GIXRD results have proved the formation of crystalline TiN phase on the surface of Sample T1 (Fig. 3), hence, the two separate peaks of N 1 s can be attributed to the Ti-N bond and N-O bond (Fig. 4b), respectively. According to the XPS database provided by the National Institute of Standards and Technology (NIST), U.S. Department of Commerce, the reported binding energy of Ti-N in TiN ranges from 396.90 eV to 397.80 eV [30]. Thus, it is possible that the green peak centralized at 397.04 eV corresponded to the Ti-N bond, while the other red peak centralized at 396.35 eV corresponded to the N-O bond. The measured O 1 s peak can also be deconvoluted to two separate peaks, with a peak value of 530.14 eV (red line) and 531.84 eV (green line), respectively (Fig. 4c). O element could form an O-Ti bond with Ti and O-N bond with N. According to the XPS database, the reported binding

energy of the O-Ti bond in TiO_2 varied from 529.70 eV to 530.20 eV. Hence, it is possible that the red peak with a peak value of 530.14 eV can be attributed to the O-Ti bond, while the other green peak belonged to the O-N bond. However, from the GIXRD results no obvious crystalline TiO_2 was detected. A possible reason was that amorphous titanium oxide was formed on the surface of Sample T1 after surface modification treatments.

From the survey spectrum of Sample T2 (Fig. 4d), it can be seen that the four elements, including Ti, O, C, and N elements, were presented on the sample surface. High-resolution spectrums of N 1 s and O 1 s are plotted separately in Fig. 4e and f, respectively. The peak of N 1 s can be deconvoluted to two separate peaks that had the same shape and size (Fig. 4e), and they were centralized at 396.15 eV (red line) and 396.76 eV (green line), respectively. The peak of N 1 s in Sample T2 (Fig. 4e) shifted to a lower value compared with that of Sample 1 (Fig. 4b). This could be ascribed to the effect of electron charging on the XPS spectrum during measurement. The ratio between the N-O bond and Ti-N bond in Sample T2 was higher than that in Sample T1, indicating that more N-O bond was formed on the surface of Sample T2 compared with that of the Sample T1 after the surface modification treatment. The peak shape of the deconvoluted O 1 s peaks of Sample T2 (Fig. 4f) was very similar to that of Sample T1 (Fig. 4c).

As can be seen from Fig. 5a, there were also four elements (Ti, O, N, and C element) detected on the surface of Sample T3. The shape of deconvoluted N 1 s peaks (Fig. 5b) was very similar to that of Sample T1. There was no significant difference of deconvoluted O 1 s peaks between Sample T3 (Fig. 5c), Sample T1, and Sample T2, except that the peak centralized value was slightly different. The XPS results of Sample T4 are demonstrated in Fig. 5 d-f. Ti, O, C, N, and Si elements were detected. Compare with the above three samples, the intensity of Ti peak was much lower, indicating that the Ti disc surface was covered by newly formed phases after the surface modification, which was in accordance with the SEM results (Fig. 2). However, Si peaks were also detected. The N 1 s peak was predominately composed of the N-O bond (Fig. 5k). Hence, the particles with polygonal morphology on Sample T4 was probably amorphous oxynitride.

Bacteriostatic Effects of the Surface-Modified Ti Discs

Sample T2, T3 and T4 were selected to carry out antibacterial tests. Meanwhile, a polished Ti disc acted as a control group. Figure 6a shows the 24-well plate loaded with the control group and tested samples for antibacterial testing. Two specimens from Sample T2, T3 and T4 were tested with the same procedure. Images of detached and re-cultivated bacteria colonies on agar plates after 100 times dilution are

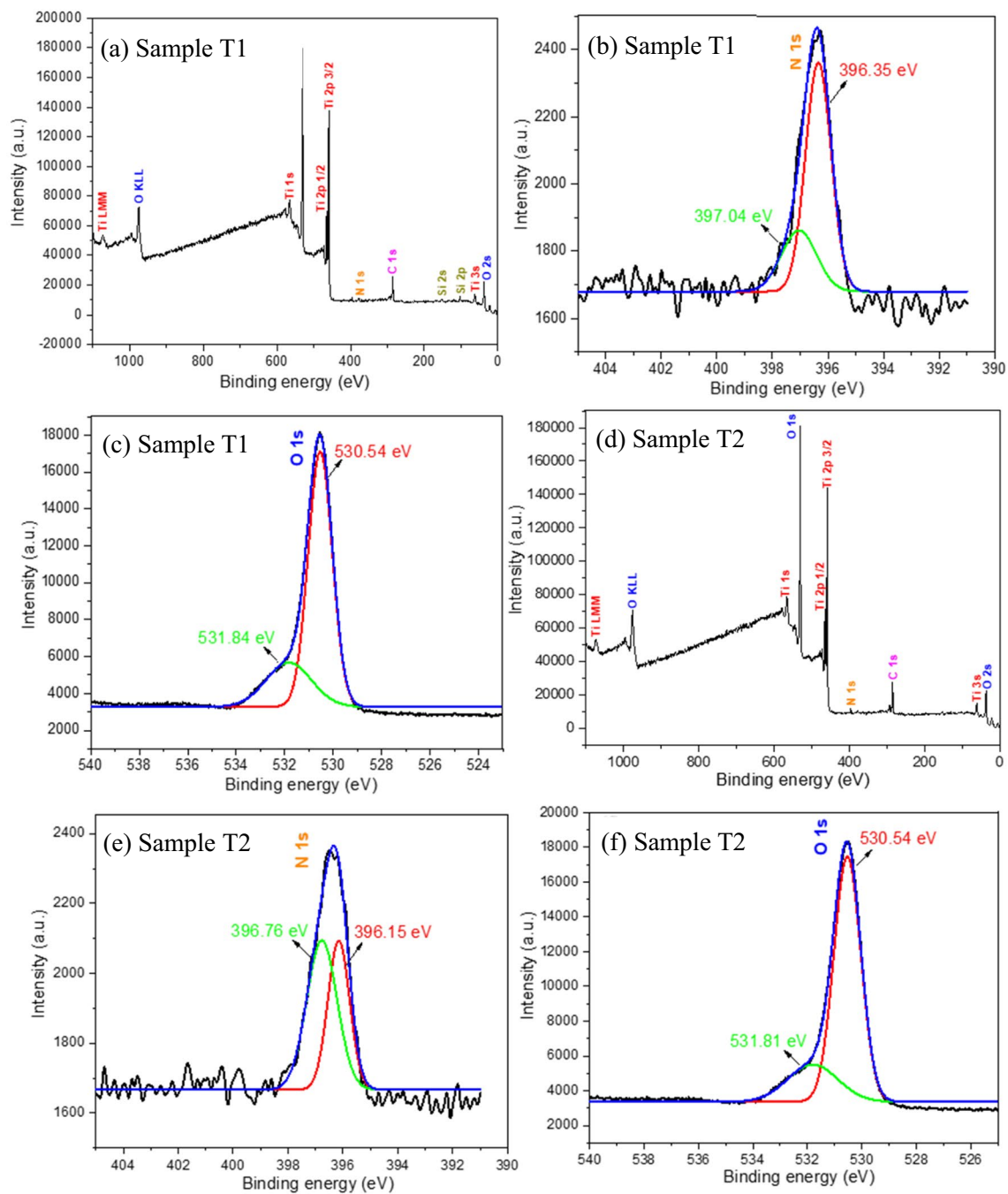


Fig. 4 XPS survey spectrum showing that Ti, O, C, N, and Si elements were detected on the surface of Sample T1 (a), and Sample T2 (d). High-resolution spectrums of N 1s and O 1s of Sample T1 (b, c) and Sample T2 (e, f)

displayed in Fig. 6b, c, from which it can be seen that the agar plate of the control group was almost fully covered by colony units. In comparison, the agar plate of Sample T2, T3, and T4 had much less colony units, indicating that the surface-modified Ti discs showed certain bacteriostatic effects compared with the unmodified Ti discs.

The total and average colony forming units, and bacterial inhibition efficiency of the tested samples are listed

in Table 2. The control group had 1608 colony forming units, whereas, the Sample T2, T3, and T4 had 427, 312, and 323 colony forming units, respectively, where were much less than the control group. The bacterial inhibition efficiency of Sample T2, T3, and T4 were calculated as 73.5%, 80.6%, and 79.9% (Table 2), respectively. Donaghy et al. created an antibacterial surface on beta Ti alloys by laser nitriding, and they found that the bacteria coverage

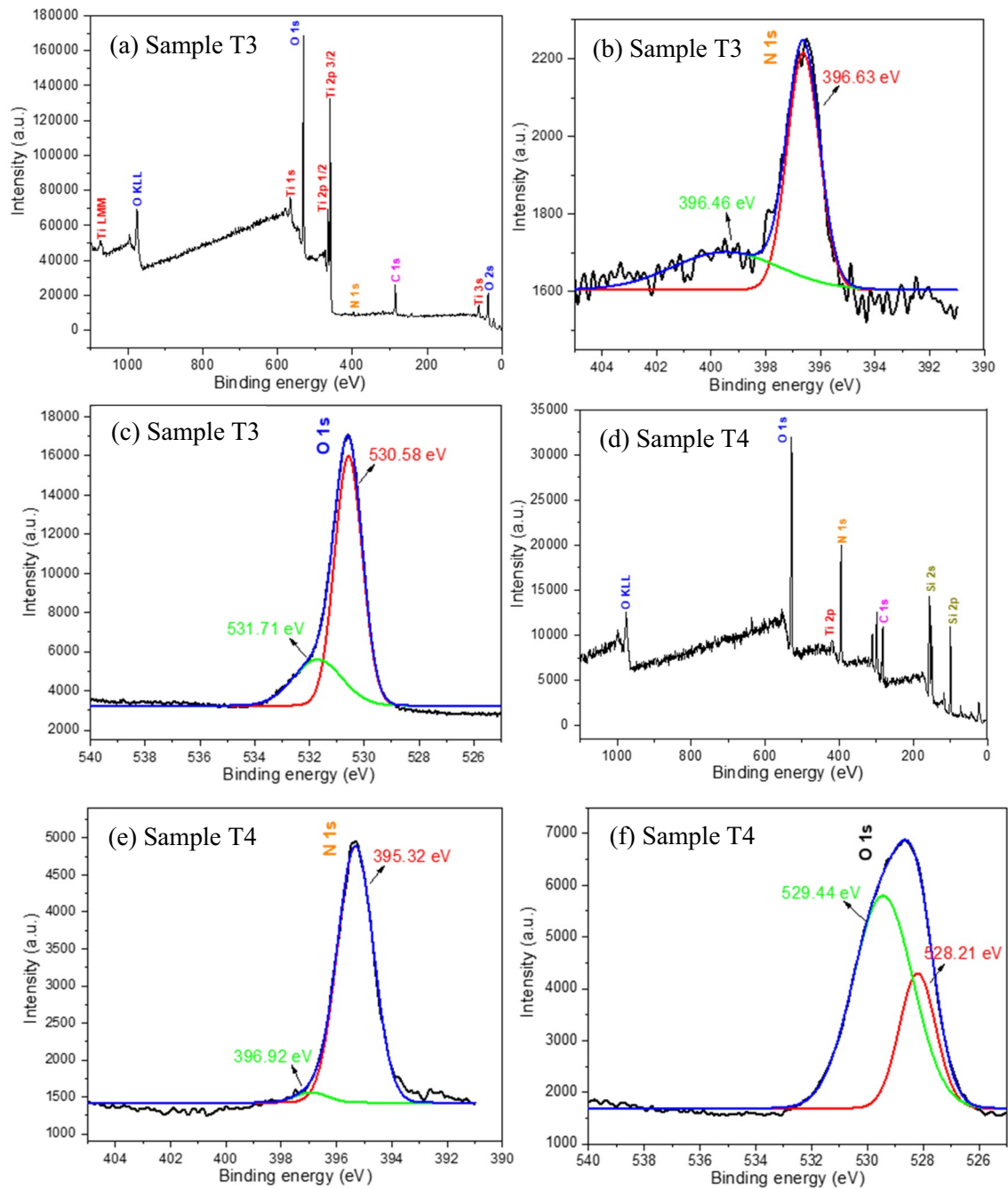


Fig. 5 XPS survey spectrum showing that Ti, O, C, N, and Si elements were detected on the surface of Sample T3 (a) and Sample T4 (d). High-resolution spectrums of N 1s and O 1s of Sample T3 (b, c) and Sample T3 (e, f)

and live-to-dead ratio of the surface-modified Ti alloys were significantly lower than those of the reference sample [23]. They attributed the antibacterial effect to the hydrophilic nature of the laser-nitrided surfaces which inhibited the attachment of hydrophobic bacteria. Chan et al. discovered that wear particles from the laser-nitrided Ti surfaces displayed antimicrobial properties against *S. aureus*, compared with those from the base metal surfaces [22].

They thought that the antibacterial activity of Ti surface was influenced by characteristics of the particles presented on the surfaces, including particle's size and shape. In the present study, we tend to believe that the bacterial inhibition of the surface-modified Ti discs was because of the formation of nitride and amorphous oxynitride. Pezzotti et al. has reported that silicon nitride ceramic can induce lysis in *porphyromonas gingivalis* and *Escherichia coli*

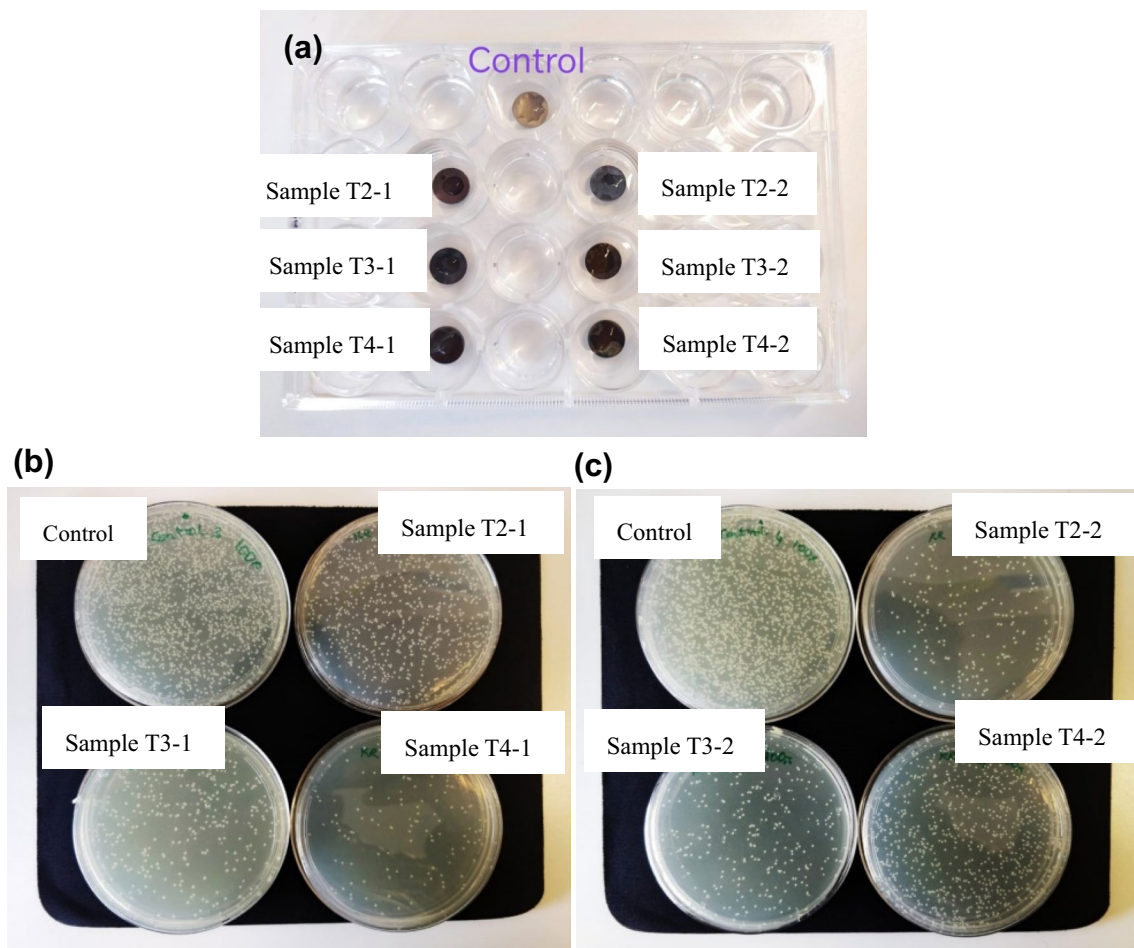


Fig. 6 Antibacterial tests. **a** 24-well plate loaded with control and test samples for antibacterial testing. **b, c** Colony forming units after incubating at 37 °C for 18 h

because of the formation of ammonium ions (and/or their modifications) [21, 22].

Herein, the nitrided Ti surfaces could release active nitrogen species when the surface-modified Ti implants were implanted into human body and interacted with human body fluid, which could impart the Ti implants with proper bacteriostatic property. In addition, the particle morphology and size on the Ti surfaces would also exert influences on

antibacterial properties. It has been shown that smaller particles have large specific surface areas and they would have greater interaction with the bacterial cell, and greater likelihood of penetration of the particle through the cell membrane [31]. Submicron and or nanoparticles were formed on the surface of Sample T1, T2, and T3, as demonstrated in Fig. 2, which might contribute to the antibacterial properties of those samples. As discussed above, several factors simultaneously exert influences on the antibacterial property of a biomaterial, including chemical composition, surface morphology, wettability, surface charge, etc. It would be difficult to separately determine how one of the above factors affect antibacterial property. In the present study, the surface-modified Ti samples after wet-chemical etching and heat-treatment under different parameters showed significant differences in terms of chemical composition (Figs. 3, 4 and 5) and surface morphology (Fig. 2). We can only qualitatively compare the bacterial inhibition effect of the samples based on the antibacterial results (Fig. 6 and Table 2). It is difficult to precisely explain why the Sample

Table 2 Total and average colony forming units, and bacterial inhibition efficiency after incubating at 37 °C for 18 h

	Control	Sample T2	Sample T3	Sample T4
Plate 1	1280	620	340	142
Plate 2	1936	234	284	504
Total	3216	854	624	646
Average	1608	427	312	323
Inhibition efficiency (%)		73.5	80.6	79.9

T3 and T4 showed higher bacterial inhibition efficiency of than Sample T2.

Merits and Limitations of the Proposed Method

Yang et al. proposed a friction stir processing strategy to incorporate Ag nanoparticles in a Ti6Al4V alloy to enhance the antibacterial property of the biomaterial [32]. They found that the bacterial inhibition efficiency of the treated Ti alloys ranged from 55 to 91% against *Staphylococcus aureus* strain and from 59 to 97% against *Escherichia coli* strain, depending on the incorporation depth of Ag nanoparticles [32]. Chan et al. utilized a laser nitriding strategy to modify the surface of Ti6Al4V alloy and they reported that the laser-nitrided Ti exhibited antibacterial activity, displaying a bacterial inhibition efficiency of 85.2% relative to the control group [22]. Lee et al. found that the Ti alloy with the addition of 10 wt% Cu showed a bacterial inhibition efficiency of 73% and the underlying mechanism was because of the production of reactive oxygen species (ROS) [1]. The bacterial inhibition efficiency of the Ti alloys processed by our surface nitriding strategy was 73.5%, 80.6%, and 79.9% for Sample T2, T3, and T4 (Table 2), respectively, which was comparable to those reported values listed above. The leading merit of our surface nitriding strategy does not lie in bacterial inhibition efficiency, but in cost and efficiency. The proposed wet-chemical etching and heat-treatment strategy is effective, simple, and cost-effective. No complicate or expensive instruments are needed, meanwhile, a large number of samples can be processed at the same time, which makes this strategy suitable for industrial production. The limitation, which could affect the applications, is the temperature we used at present. Lower temperature and short holding time could largely decrease the treating effect on the titanium substrate, i.e., the possible effect on mechanical properties. Future work will be performed using different gases and lowering the treating temperature.

Conclusions

In this study, the surface of Ti discs was nitrided by a relatively simple process. The phase composition and morphology of newly formed phases on the sample surface were investigated by GIXRD, SEM and XPS. The selection of etching chemicals and thermal treatment parameters showed the significant effects on the phase composition and morphology of the sample surface. Meanwhile, crystalline oxide, nitride, and amorphous oxynitride were detected on the surface-modified Ti discs. Antibacterial tests indicated that the surface-modified Ti discs had obvious bacterial inhibition effect compared with the non-treated Ti discs. The bacterial inhibition effect was attributed to the released reactive

nitrogen species from the Ti surfaces. The combination of wet-chemical etching and thermal treatment is an effective and simple surface modification strategy to enhance the antimicrobial properties of Ti alloy biomaterials.

Acknowledgements Dr. Xia acknowledges the financial support of the Swedish research council (2021-05626) and STINT foundation (CH2020-8762).

Author Contributions LF: methodology, data analysis, writing original draft. KR: Part of experiments, review & editing. IK: XPS analyses, review & editing. YL: antibacterial analyses. HW: Supervision, antibacterial analyses, review & editing. HE: supervision, review & editing. WX: Idea, supervision, part of experiments, review & editing, project administration.

Funding Open access funding provided by Uppsala University. This study was supported by Swedish Research Council (Grant No. 2021-05626), STINT Foundation (Grant No. CH2020-8762).

Data Availability The data that support the findings of this study are available from the corresponding author (Wei Xia) on reasonable request

Declarations

Conflict of interest The authors declare that they have no known competing financial interests or personal relationships that could have appeared to influence the work reported in this paper.

Open Access This article is licensed under a Creative Commons Attribution 4.0 International License, which permits use, sharing, adaptation, distribution and reproduction in any medium or format, as long as you give appropriate credit to the original author(s) and the source, provide a link to the Creative Commons licence, and indicate if changes were made. The images or other third party material in this article are included in the article's Creative Commons licence, unless indicated otherwise in a credit line to the material. If material is not included in the article's Creative Commons licence and your intended use is not permitted by statutory regulation or exceeds the permitted use, you will need to obtain permission directly from the copyright holder. To view a copy of this licence, visit <http://creativecommons.org/licenses/by/4.0/>.

References

1. L. Fowler, O. Janson, H. Engqvist, S. Norgren, C. Öhman-Mägi, Antibacterial investigation of titanium-copper alloys using luminescent *Staphylococcus epidermidis* in a direct contact test. *Mater. Sci. Eng. C*. **97**, 707–714 (2019). <https://doi.org/10.1016/j.msec.2018.12.050>
2. M. Chen, L. Yang, L. Zhang, Y. Han, Z. Lu, G. Qin, E. Zhang, Effect of nano/micro-Ag compound particles on the bio-corrosion, antibacterial properties and cell biocompatibility of Ti-Ag alloys. *Mater. Sci. Eng. C*. **75**, 906–917 (2017). <https://doi.org/10.1016/j.msec.2017.02.142>
3. J.W. Costerton, P.S. Stewart, E.P. Greenberg, Bacterial biofilms: a common cause of persistent infections. *Science* **284**, 1318–1322 (1999). <https://doi.org/10.1126/science.284.5418.1318>
4. L. Fu, Y. Xiong, G. Carlsson, M. Palmer, S. Örn, W. Zhu, X. Weng, H. Engqvist, W. Xia, Biodegradable Si₃N₄ bioceramic sintered with Sr, Mg and Si for spinal fusion: Surface characterization and biological evaluation. *Appl. Mater. Today*. **12**, 260–275 (2018). <https://doi.org/10.1016/j.apmt.2018.06.002>

5. G. Jin, H. Qin, H. Cao, S. Qian, Y. Zhao, X. Peng, X. Zhang, X. Liu, P.K. Chu, Synergistic effects of dual Zn/Ag ion implantation in osteogenic activity and antibacterial ability of titanium. *Biomaterials* **35**, 7699–7713 (2014). <https://doi.org/10.1016/j.biomaterials.2014.05.074>
6. R. López-Píriz, B. Cabal, L. Goyos-Ball, A. Fernández, J.F. Bartolomé, J.S. Moya, R. Torrecillas, Current state-of-the-art and future perspectives of the three main modern implant-dentistry concerns: Aesthetic requirements, mechanical properties, and peri-implantitis prevention. *J. Biomed. Mater. Res. - Part A*. (2019). <https://doi.org/10.1002/jbm.a.36661>
7. L. Kunčická, R. Kocich, T.C. Lowe, Advances in metals and alloys for joint replacement. *Prog. Mater. Sci.* **88**, 232–280 (2017). <https://doi.org/10.1016/j.pmatsci.2017.04.002>
8. L.C. Zhang, L.Y. Chen, L. Wang, Surface modification of titanium and titanium alloys: technologies, developments, and future interests. *Adv. Eng. Mater.* **22**, 1–37 (2020). <https://doi.org/10.1002/adem.201901258>
9. F. Rupp, L. Liang, J. Geis-Gerstorfer, L. Scheideler, F. Hüttig, Surface characteristics of dental implants: a review. *Dent. Mater.* **34**, 40–57 (2018). <https://doi.org/10.1016/j.dental.2017.09.007>
10. D. Guadarrama Bello, A. Fouillen, A. Badia, A. Nanci, A nanoporous titanium surface promotes the maturation of focal adhesions and formation of filopodia with distinctive nanoscale protrusions by osteogenic cells. *Acta Biomater.* **60**, 339–349 (2017). <https://doi.org/10.1016/j.actbio.2017.07.022>
11. A.S.D. Al-Radha, D. Dymock, C. Younes, D. O'Sullivan, Surface properties of titanium and zirconia dental implant materials and their effect on bacterial adhesion. *J. Dent.* **40**, 146–153 (2012). <https://doi.org/10.1016/j.jdent.2011.12.006>
12. D.H. Song, S.H. Uhm, S.B. Lee, J.G. Han, K.N. Kim, Antimicrobial silver-containing titanium oxide nanocomposite coatings by a reactive magnetron sputtering. *Thin Solid Films* **519**, 7079–7085 (2011). <https://doi.org/10.1016/j.tsf.2011.01.385>
13. H. Cao, F. Meng, X. Liu, Antimicrobial activity of tantalum oxide coatings decorated with Ag nanoparticles. *J. Vac. Sci. Technol. A Vac. Surf. Film.* **34**, 04C102 (2016). <https://doi.org/10.1116/1.4947077>
14. C. Larsson, P. Thomsen, B.O. Aronsson, M. Rodahl, J. Lausmaa, B. Kasemo, L.E. Ericson, Bone response to surface-modified titanium implants: Studies on the early tissue response to machined and electropolished implants with different oxide thicknesses. *Biomaterials* **17**, 605–616 (1996). [https://doi.org/10.1016/0142-9612\(96\)88711-4](https://doi.org/10.1016/0142-9612(96)88711-4)
15. G.P. Rodriguez, G. Herranz, A. Romero, Solar gas nitriding of Ti6Al4V alloy. *Appl. Surf. Sci.* **283**, 445–452 (2013). <https://doi.org/10.1016/j.apsusc.2013.06.128>
16. K. Fujita, M. Ijiri, Y. Inoue, S. Kikuchi, Rapid nitriding of titanium alloy with fine grains at room temperature. *Adv. Mater.* (2021). <https://doi.org/10.1002/adma.202008298>
17. G. Pezzotti, R.M. Bock, B.J. McEntire, E. Jones, M. Boffelli, W. Zhu, G. Baggio, F. Boschetto, L. Puppulin, T. Adachi, T. Yamamoto, N. Kanamura, Y. Marunaka, B.S. Bal, Silicon nitride bioceramics induce chemically driven lysis in porphyromonas gingivalis. *Langmuir* **32**, 3024–3035 (2016). <https://doi.org/10.1021/acs.langmuir.6b00393>
18. G. Pezzotti, A spontaneous solid-state NO donor to fight antibiotic resistant bacteria. *Mater. Today Chem.* **9**, 80–90 (2018). <https://doi.org/10.1016/j.mtchem.2018.05.004>
19. E. Marin, F. Boschetto, M. Zanocco, W. Zhu, T. Adachi, N. Kanamura, T. Yamamoto, B.J. McEntire, E.N. Jones, C. Powell, J. Hendry, R.M. Bock, B.S. Bal, G. Pezzotti, Biological responses to silicon and nitrogen-rich PVD silicon nitride coatings. *Mater. Today Chem.* **19**, 100404 (2021). <https://doi.org/10.1016/j.mtchem.2020.100404>
20. X. Hu, S. Mei, F. Wang, S. Tang, D. Xie, C. Ding, W. Du, J. Zhao, L. Yang, Z. Wu, J. Wei, A microporous surface containing Si₃N₄/Ta microparticles of PEKK exhibits both antibacterial and osteogenic activity for inducing cellular response and improving osseointegration. *Bioact. Mater.* **6**, 3136–3149 (2021). <https://doi.org/10.1016/j.bioactmat.2021.02.027>
21. L. Li, J. Gao, G. Chang, J. Mu, E. Xu, X. Liu, J. Yan, H. Zhou, L. Zhang, Effect of β-SiAlON content on the sintering and bacteriostatic properties of β-SiAlON–Si₃N₄ composite ceramics. *Ceram. Int.* **48**, 33704–33711 (2022). <https://doi.org/10.1016/j.ceramint.2022.07.316>
22. C.W. Chan, J. Quinn, I. Hussain, L. Carson, G.C. Smith, S. Lee, A promising laser nitriding method for the design of next generation orthopaedic implants: Cytotoxicity and antibacterial performance of titanium nitride (TiN) wear nano-particles, and enhanced wear properties of laser-nitrided Ti6Al4V surfaces. *Surf. Coatings Technol.* **405**, 126714 (2021). <https://doi.org/10.1016/j.surfcoat.2020.126714>
23. C. Lubov Donaghy, R. McFadden, S. Kelaini, L. Carson, A. Margariti, C.W. Chan, Creating an antibacterial surface on beta TNZT alloys for hip implant applications by laser nitriding. *Opt. Laser Technol.* **121**, 105793 (2020). <https://doi.org/10.1016/j.optlastec.2019.105793>
24. X. Zong, H. Wang, J. Li, X. Cheng, Z. Li, H. Tang, Microstructure characterization and evolution mechanism of titanium during laser surface nitriding. *Mater. Charact.* **190**, 112029 (2022). <https://doi.org/10.1016/j.matchar.2022.112029>
25. R.M. Bock, B.J. McEntire, B.S. Bal, M.N. Rahaman, M. Boffelli, G. Pezzotti, Surface modulation of silicon nitride ceramics for orthopaedic applications. *Acta Biomater.* **26**, 318–330 (2015). <https://doi.org/10.1016/j.actbio.2015.08.014>
26. D.J. Gorth, S. Puckett, B. Ercan, T.J. Webster, M. Rahaman, B. Sonny Bal, Decreased bacteria activity on Si₃N₄ surfaces compared with PEEK or titanium. *Int. J. Nanomed.* **7**, 4829–4840 (2012). <https://doi.org/10.2147/IJN.S35190>
27. X. Zong, H. Wang, Z. Li, J. Li, X. Cheng, Y. Zhu, X. Tian, H. Tang, Laser nitridation on Ti-6.5Al-3.5Mo-1.5Zr-0.3Si titanium alloy. *Surf. Coat. Technol.* **386**, 125425 (2020). <https://doi.org/10.1016/j.surfcoat.2020.125425>
28. L.C. Xu, M.E. Meyerhoff, C.A. Siedlecki, Blood coagulation response and bacterial adhesion to biomimetic polyurethane biomaterials prepared with surface texturing and nitric oxide release. *Acta Biomater.* **84**, 77–87 (2019). <https://doi.org/10.1016/j.actbio.2018.11.035>
29. O. Sakata, M. Nakamura, Grazing Incidence X-Ray Diffraction, in *Surf Sci Tech.* ed. by G. Bracco, B. Holst (Springer, Berlin, 2013), pp.165–190
30. XPS Database, National Institute of Standards and Technology (NIST), U.S. Department of Commerce, <https://srdata.nist.gov/xps/selectEnergyType.aspx>, (n.d.).
31. L. Wang, C. Hu, L. Shao, The antimicrobial activity of nanoparticles: present situation and prospects for the future. *Int. J. Nanomed.* **12**, 1227–1249 (2017). <https://doi.org/10.2147/IJN.S121956>
32. Z. Yang, H. Gu, G. Sha, W. Lu, W. Yu, W. Zhang, Y. Fu, K. Wang, TC4/Ag metal matrix nanocomposites modified by friction stir processing: surface Characterization, antibacterial property, and cytotoxicity in vitro. *ACS Appl. Mater. Interfaces* **10**, 41155–41166 (2018)